

NASA Technical Memorandum 106719  
AIAA-94-2690

10-07  
20519  
20P

# Inlet Flow Test Calibration for a Small Axial Compressor Facility Part I—Design and Experimental Results

D.P. Miller  
*Lewis Research Center*  
*Cleveland, Ohio*

(NASA-TM-106719) INLET FLOW TEST  
CALIBRATION FOR A SMALL AXIAL  
COMPRESSOR FACILITY. PART 1: DESIGN  
AND EXPERIMENTAL RESULTS (NASA.  
Lewis Research Center) 20 p

N95-11005

Unclas

G3/07 0020318

and

P.S. Prahst  
*NYMA, Inc.*  
*Engineering Services Division*  
*Brook Park, Ohio*

Prepared for the  
30th Joint Propulsion Conference  
cosponsored by AIAA, ASME, SAE, and ASEE  
Indianapolis, Indiana, June 27-29, 1994



National Aeronautics and  
Space Administration



**Inlet Flow Test Calibration for a Small  
Axial Compressor Facility  
Part I. Design and Experimental Results**

**D. P. Miller<sup>†</sup>  
NASA Lewis Research Center  
Cleveland, OH 44135**

**P. S. Prahst<sup>‡</sup>  
NYMA, Inc.  
Cleveland, OH 44135**

**Abstract**

An axial compressor test rig has been designed for the operation of small turbomachines. The inlet region consisted of a long flowpath region with two series of support struts and a flapped Inlet Guide Vane. A flow test was run to calibrate and determine the source and magnitudes of the loss mechanisms in the inlet for a highly loaded two-stage axial compressor test. Several flow conditions and IGV angle settings were established in which detailed surveys were completed. Boundary layer bleed was also provided along the casing of the inlet behind the support struts and ahead of the IGV. A detailed discussion of the flowpath design along with a summary of the experimental results are provided in Part I.

**1.0 Introduction**

NASA Lewis Research Center has several facilities dedicated to compressor research. One of the facilities designated to small compressor research is the SECTF[1], Small Engine Components Test Facility. The facility, shown in Figure 1, was designed to handle flows up to 30 kg/s, a maximum pressure ratio of 30:1, provide a maximum speed of 60,000 rpm and produce a maximum shaft horsepower of 6000. Compressor inlet air can be varied from 2 to 50 psia and the air temperature varied from ambient to -57 C. The test was conducted using atmospheric inlet conditions.

**Small Engine Components Compressor Test Facility**

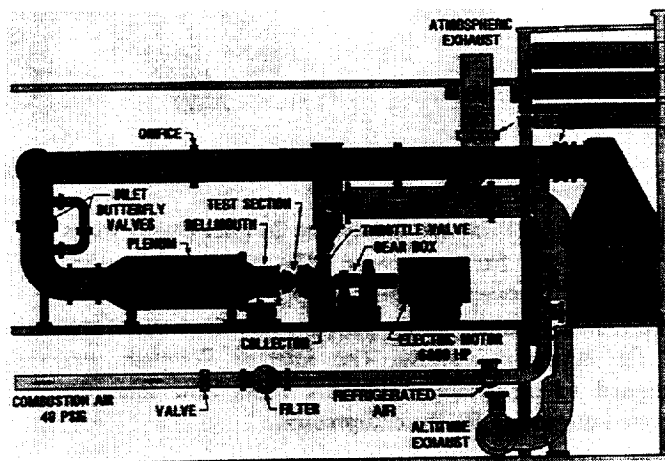


**Figure 1: CE18 Test Facility at NASA Lewis**

A joint cooperative program with Allison Gas Turbine was established to run a small highly loaded axial compressor in the facility. In order to establish a baseline flow through the inlet which will be used for the compressor test, a flow test without the compressor was conducted to survey the inlet region ahead of the compressor face. Details of the flowpath design will be presented later in this paper. As indicated by Figure 2, the inlet region consisted of a bellmouth (not actually shown) connected to a 36 cm bullet nose. The inlet included 5 small support struts approximately 13 cm downstream of the leading edge of the bullet nose, 5 main support struts at

<sup>†</sup>Member AIAA  
<sup>‡</sup>Member ASME

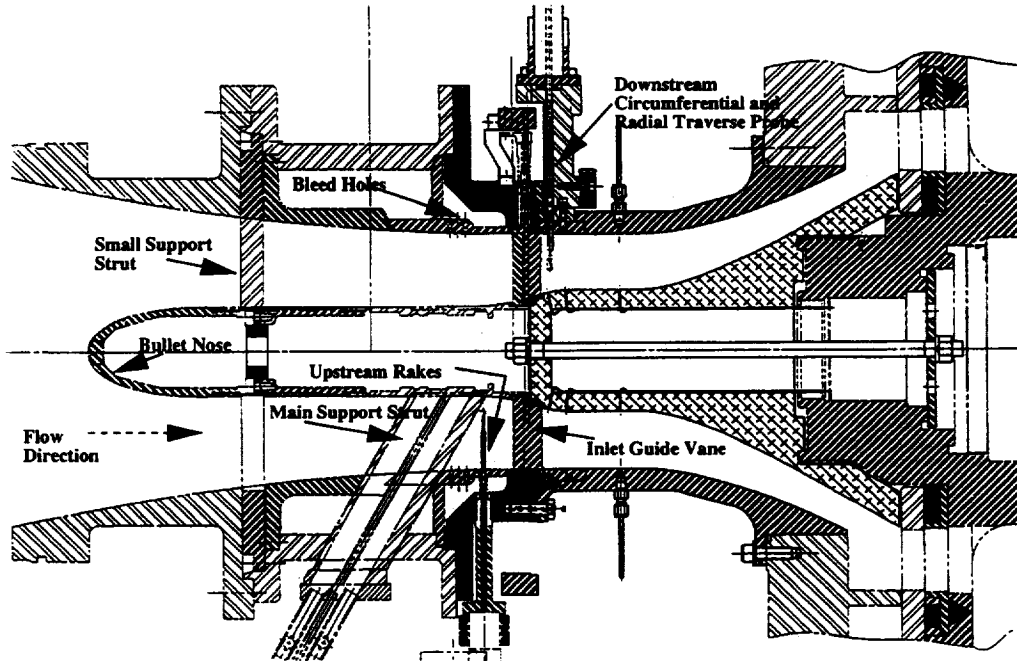


**Figure 2: Cross Sectional View of the Cold Flow Configuration**

approximately 28 cm and finally, the 26 Inlet Guide Vanes around 36 cm from the nose. The small struts were staggered in between the main support struts. This was done to minimize the losses generated by the wakes from all the supporting struts. The internal flowpath was designed to pass 10% additional mass flow than the targeted mass flow for the compressor.

## 2.0 Instrumentation

### 2.1 Miniature Flow Measuring Probe

To obtain detailed flow information, the flow test configuration was instrumented with a radial and tangential traverse miniature flow measuring probe at approximately 1 cm downstream of the Inlet Guide Vane. This distance downstream of the IGV was equivalent to the downstream leading edge of the compressor first stage rotor. Figures 3a and 3b show the miniature probe design which measured total temperature and pressure, along with being able to yaw to find flow angle by balancing the static pressures on the sides of the probe. The probe was designed to have 0.051 cm diameter pressure tubing and the actuator to have a radial travel of over 5.1 cm and circumferential travel of  $74^\circ$ . The probe actuator was designed with a large tangential travel to measure all the wakes from the upstream struts, instrumentation and Inlet Guide Vanes.

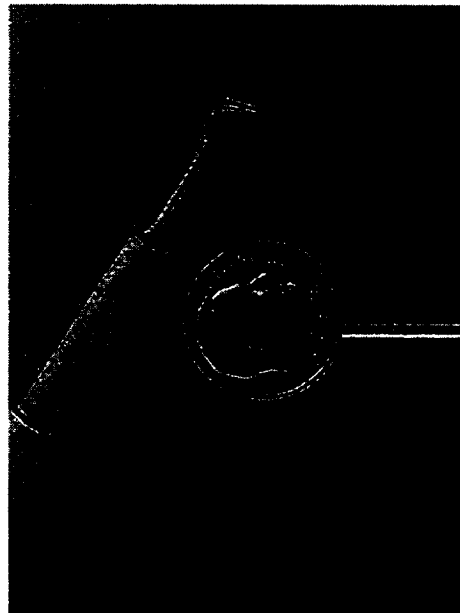


**Figure 3a: View of the Miniature Measurement Probe**



**Figure 3b: Close Up View of the Probe**

## 2.2 Fixed Rakes

Ahead of the Inlet Guide Vanes, five fixed rakes were used which consisted of 5 total temperature and total pressure elements on the same rake, Figure 4. The rake was constructed with 0.081 cm diameter pressure tubing and shielded thermocouples for total temperature measurements with a radial length of over 5.1 cm and 0.274

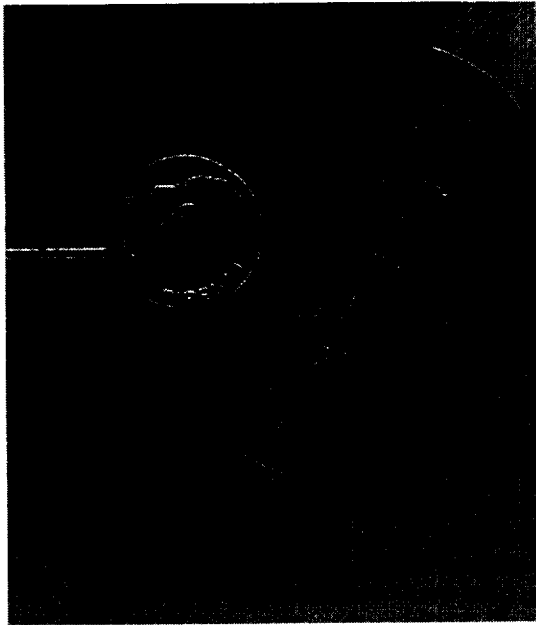


**Figure 4: Inlet Fixed Rakes Ahead of the IGV**

cm total width. The inlet rakes were provided to assess the difference between the plenum total conditions and the total conditions ahead of the Inlet Guide Vanes.

## 2.3 Static Pressure Measurements

Finally, there were several static pressure taps located on the outer diameter and the inner diameter of the flowpath. The static pressures were included to verify the design intent for the flowpath geometry. The static pressures were located at the trailing edge of the main support strut, at the downstream measurement plane and two more positions aft of the measuring plane. There were at least six circumferential locations for each axial position of the static tap.

## 3.0 Aerodynamical Design of the Hardware

### 3.1 Inlet Flowpath Region

The inlet region consists of the bellmouth up to and including the Inlet Guide Vane. The facility was designed with a large plenum tank ahead of the compressor leading to a bellmouth region in front of the compressor. The bellmouth was designed for small compressor flow sizes and the inlet was designed for the scaled NASA 3-stage compressor[2]. The bullet nose design was partially a result of the mechanical design and the aerodynamics. Since the long bellmouth produced a slowly accelerating flow field, the bullet nose was designed to maintain a constant acceleration which would establish a positive pressure gradient and keep the boundary layer development relatively small compared to the height of the annulus. For mechanical considerations, the original nose had to be lengthened to accommodate instrumentation or a slip ring inside the front of the nose and a small strut added for support. The coordinates of the inlet geometry for the flowpath can be found in Appendix A.1.0. Additionally, bleed holes were added just ahead of the IGV along the casing to allow boundary layer bleed. The bleed holes were designed to remove up to 10% mass flow.

### 3.2 Inlet Small Support Strut Design

As mentioned above the bullet nose was lengthened to accommodate some instrumentation or a slip ring, but further structural analysis indicated that the nose would not be rigid enough to handle various vibrational modes the nose would be subjected to. As a consequence of the analysis, 5 small support struts were added to the inlet about 13 cm downstream of the leading edge of the bullet nose. The chord length of the strut was fixed at 1.91cm. To minimize the effect of the strut, a NACA0024 thick

symmetrical airfoil[3], was chosen because the strut needed to have a maximum thickness to chord of 24% to maintain structural integrity and minimize inlet distortions. The struts were placed circumferentially in between the main support struts' circumferential locations. The airfoil coordinates can be found in Appendix A.1.1.

### 3.3 Inlet Main Support Strut Design

As part of the original inlet design, five main support struts were needed, to provide structural support of the inlet inner housing, and to provide some services running through the strut. For example, oil lines were needed to provide lubrication of the bearings and return scavenge lines. Another strut was used to run static pressure lines to the inner flowpath. Therefore, the struts had to be a specific chord length and thickness to provide services and support. Given the struts had to be 6.35 cm in chord length with a maximum thickness to chord ratio of 14%, an inverse design method developed by Jose Sanz[4] was used to obtain the aerodynamic shape. The final aerodynamic shape along with the coordinates are found in Appendix A.1.2.

### 3.4 Inlet Guide Vanes

The Inlet Guide Vanes are a scaled down version of a NASA 5-stage compressor[2]. The IGV was designed with a 2% total pressure drop and modeled from a cascade airfoil using a (DCA) double circular arc shape with no camber. The aerodynamic shape along with the coordinates are found in Appendix A.1.3.

### 3.5 Main Flowpath Region

The flowpath region aft of the inlet was designed using a new design system developed at NASA Lewis Research Center[5]. Traditionally, an inviscid axisymmetric streamline curvature program would have been used to specify the flowpath, and a boundary layer computation performed afterwards. The new system computes the viscous throughflow and thus provides the designer with greater freedom to modify the geometry and make the computation. This approach was used to design the main flowpath region between the IGVs and the collector.

Since the inlet was designed for small flow size compressors, the main flowpath needed to be designed to flow 10% more mass flow than the targeted flow for the scaled 3-Stage compressor or the Allison multi-stage compressor. The design mass flow was determined to be around 5 kg/s. The design of the flowpath was constrained by two fixed points on the collector. The first hard point was located on the inner diameter of the collector. The second point was on the outer diameter of the collector

leading to the throttle valve which constrained the outer maximum diameter of the main flowpath. The new flowpath was designed to maintain a constant acceleration through the inlet and to the compressor face. From the compressor face it was desirable to maintain a constant Mach number throughout the flow field to maximize the flow rate, however, due to the fixed hard points on the collector, the area decreases. The area decrease produced an accelerating flow field which develops a favorable pressure gradient minimizing the boundary layer which prevents the flow from choking in the flowpath. The decrease in area did limit the maximum flow capacity the test could pass. The maximum 1-D flow based upon standard day inlet conditions and minimum area from the flowpath design was determined by the following,

Choked Mass Flow Conditions:

$$\dot{m}^* = A_t P_0 \frac{\gamma}{\sqrt{\gamma R T_0}} \left( \frac{2}{\gamma + 1} \right)^{\frac{(\gamma + 1)}{2(\gamma - 1)}} \quad (1)$$

where

$\dot{m}^*$   $\equiv$  Critical Mass Flow

$A_t$   $\equiv$  Throat Area

$P_0$   $\equiv$  Plenum Stagnation Pressure

$T_0$   $\equiv$  Plenum Stagnation Temperature

$\gamma$   $\equiv$  Specific Heat Ratio

$R$   $\equiv$  Universal Gas Constant

Therefore, for standard day conditions the maximum critical mass flow for the flowpath design was calculated to be

$$\dot{m}^* = 5.2 \text{ kg/sec}$$

The flow for the flowpath design was computed with a viscous through flow code (VIADAC)[5] and the maximum computed flow with boundary layer blockage was determined to be

$$\dot{m}^* = 5.0 \text{ kg/sec}$$

The final main flowpath design was determined after several iterations using the viscous flow code. The code was used to examine boundary layer growth and determine smoothness of the geometry for any large diffusion areas or separations which might have occurred in the original design. The coordinates for the flowpath can be found in Appendix A.1.4.

#### 4.0 Experimental Results

The test rig was assembled in the SECTF at NASA Lewis and the throttle valve set to full open position. The flow was established in the rig by applying altitude exhaust to the exit. This would hopefully choke the flow stream somewhere in the main flowpath duct, however, the throttle area was determined to be smaller than the main flowpath, hence, the flow would choke in the throttle valve first, and this established the maximum flow. The throttle valve was designed as a disk with slots. The throat area of the throttle valve was calculated to be  $A_t = 284 \text{ cm}^2$ . The design of the throttle valve resembles an orifice. Upon examination of orifice designs[6], the discharge coefficient for the design was found to be  $C_d = 0.61$ . The effective throat area for the valve was  $A_{eff} = C_d A_t$ . The maximum flow at Standard Day Conditions from equation 1.0 becomes

$$\dot{m}_{throttle}^* = 4.2 \text{ kg/sec}$$

The throttle valve set the maximum flow at all positions and not the design of the flowpath.

#### 4.1 Cold Flow Test Conditions

The following set of conditions were established to take detailed flow measurements downstream of the IGV.

The range of flow test conditions, as indicated in Table 1, was chosen which typifies operating conditions an actual

**Table 1: Range of Flow Test Conditions**

$\dot{m} \sqrt{\theta/\delta}$	IGV $\alpha$	%Bleed
3.86	0.0	0.0
3.86	0.0	2.0
3.27	30.0	0.0
3.27	30.0	4.0

compressor might experience during a test.

$\dot{m} \equiv$  Mass Flow

$\theta \equiv T_0 / T_{0std}$

$\delta \equiv P_0 / P_{0std}$

$\alpha \equiv$  Angle in Degrees

The maximum corrected flow the rig could experience was roughly 3.86 kg/s due to testing with atmospheric inlet conditions during the colder months at NASA Lewis Research Center.

The miniature traversing probe was designed to produce a full traverse of 74 degrees. The home position was located at 270 degrees (top dead center 0 degrees aft looking forward) and the probe could automatically traverse in the theta direction towards 342 degrees. To determine the amount of circumferential data to be taken at each radii, reference locations had to be determined for the IGVs, Small Support Struts, Main Support Struts and Inlet Rakes. The reference locations serve as a guide to setting the traverse probe position in theta to obtain as much detailed wake information as necessary to make as accurate as possible the loss computations of the data. Table 2 shows the reference theta locations for the various struts and IGVs where the probe will be traversed.

**Table 2: Reference Theta Locations for Objects to be Traversed**

Object	Theta Location	Ref. Theta Location
IGV	270.000	0.00
IGV	283.846	13.846
Inlet Rake	285.460	15.767
Small Strut	288.000	18.000
IGV	297.692	27.692
IGV	311.538	41.538
Main Strut	324.000	54.000
IGV	325.385	55.385
IGV	339.230	69.230
Stop Traverse	342.000	72.000

These approximately locate the wakes associated with each object in the flow stream. The plane was first traversed to find the actual wake locations and then the circumferential positioning was refined. The wakes moved each time the IGV was moved to a new turning angle position and the process had to be repeated.

With the wake locations established, the probe was traversed radially. The height of the traversing plane was 5.029 centimeters. Thus, the minimum radial location was around 0.036 cm from the hub, which represents about 99% immersion or 1% span of the duct. Table 3 indicates the radii chosen for a radial traverse at a fixed theta location to obtain the radial flow profile. Most of the radii were used to map the entire flowfield in both directions with exceptions to 0, 3, 99 and 100% immersions.

**Table 3: Reference Radial Positions for the Miniature Traverse Probe**

Radius(cm)	Height	%Span	%Imm
9.9568	5.0292	100	0
9.8044	4.8768	97	3
9.7053	4.7777	95	5
9.5758	4.6482	92	8
9.4539	4.5263	90	10
8.9510	4.0233	80	20
8.4480	3.5204	70	30
7.9451	3.0175	60	40
7.4422	2.5146	50	50
6.9393	2.0117	40	60
6.4364	1.5088	30	70
5.9334	1.0058	20	80
5.4305	0.5029	10	90
5.1791	0.2515	5	95
5.0282	0.1006	2	98
4.9784	0.0508	1	99
4.9276	0.0000	0	100

#### 4.2 Test Data Results

For all the results shown, the measured total pressure is normalized with the plenum total pressure. Rakes were inserted upstream of the inlet guide vanes (IGVs) to measure temperature and pressure radial profiles, and to obtain inlet conditions. The rakes were composed of five radial elements equally spaced circumferentially. Figure 5 shows the normalized total pressure and temperature ratios of the rake elements as a function of spanwise location. The average rake values were found to be less than 0.2% in error from the plenum conditions.

Radial and circumferential surveys were then taken behind the inlet guide vane with a traversing miniature cobra probe at the maximum corrected flowrate for the cold flow test. Contours of the total pressures measured behind the inlet guide vanes set at 0 degrees and 0% bleed are shown in Figure 6a. With the inlet rakes left in the flowfield, the probe was traversed over the 72° sector of the flow. The pressure contours indicate definite wakes shed

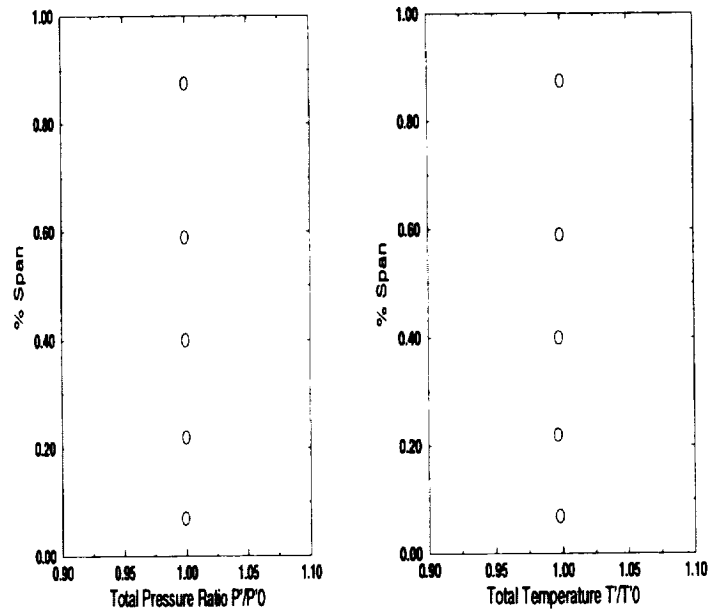


**Figure 5: Spanwise variation of Normalized Pressure and Temperature Ratios for the Inlet Rakes.**

from the grouping of the inlet rake, the IGV and a small strut. The main strut wake is also visible in the flowfield behind the IGV as well. There is evidence of the boundary layer along the shroud, and the hub region also shows a small boundary layer. Figures 6b and 6c show the flow angle and Mach number contours at the IGV exit. The Mach numbers vary from 0.38 in the wake region to 0.48 in the core flow region. The Mach number in the core is higher nearer the hub due to the converging inner flowpath.

After comparing the inlet rake data to the plenum conditions and finding insignificant differences between these measurements, the rakes were removed from the flow and the conditions were repeated without the upstream rakes. Figure 7a shows the contours of the total pressure ratio without the presence of the inlet rakes. The area where the inlet rake was located is now showing a wake only cast by the inlet guide vane, the small strut upstream does not impact the flow at all. The flow angle contours and Mach number contours without the rakes can be found in Figures 7b and 7c.

From the flow angle measurement it becomes obvious that the inlet rake caused a considerable disturbance in the flow stream while the small inlet strut has no significant impact. The performance substantially improved by removing the inlet rake.

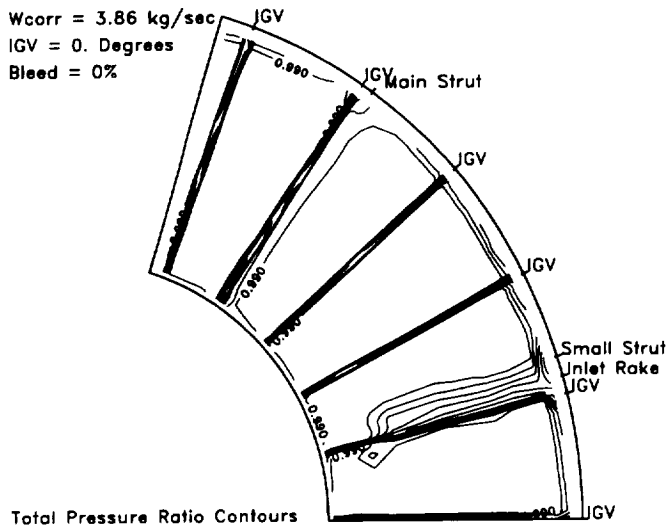


Figure 6a: Total pressure ratio contours, ranging from 0.93 to 0.99 in intervals of 0.01

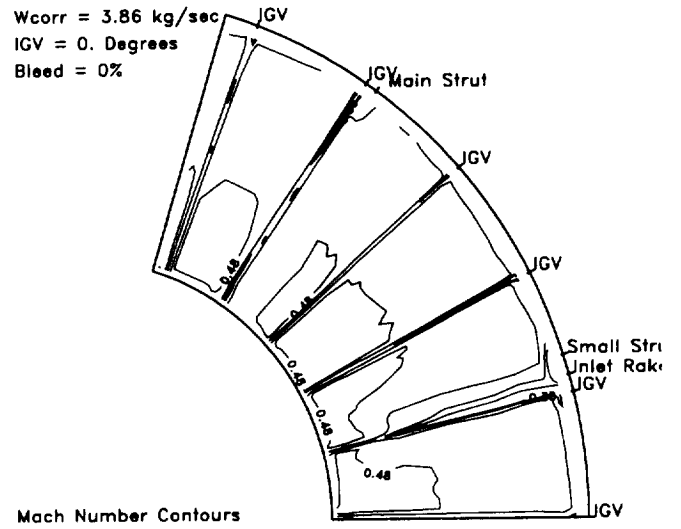


Figure 6c: Mach number contours, ranging from 0.34 to 0.48 in intervals of 0.02

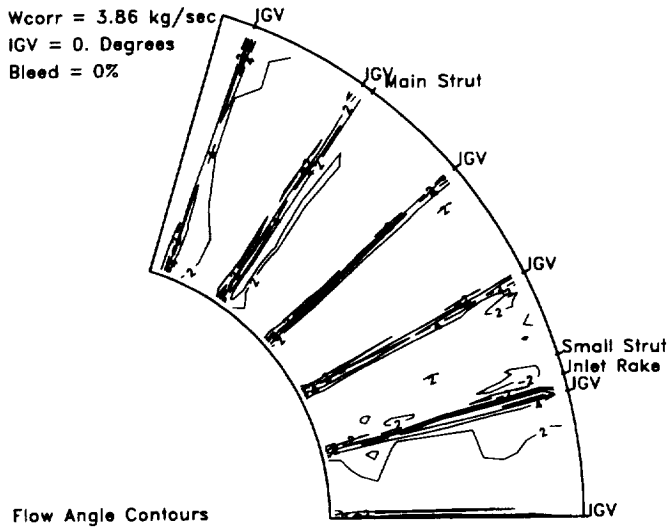


Figure 6b: Exit flow angle contours, ranging from -6 to 8 degrees in intervals of 2 degrees

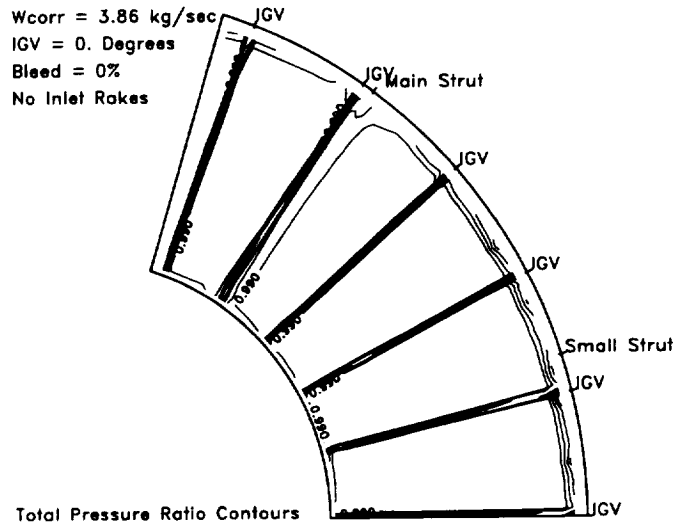
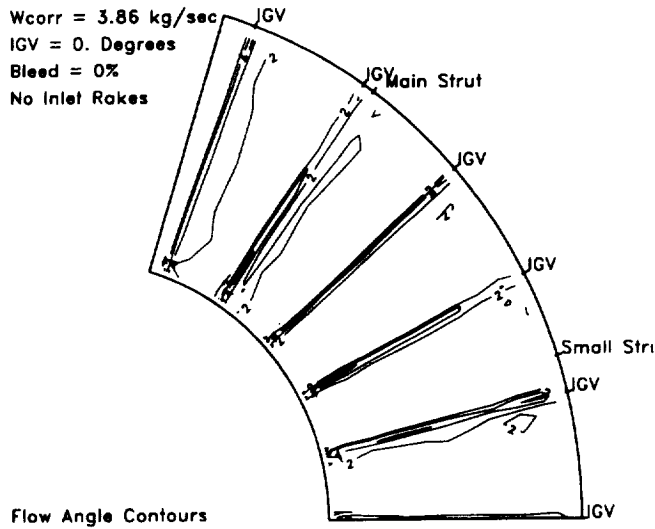
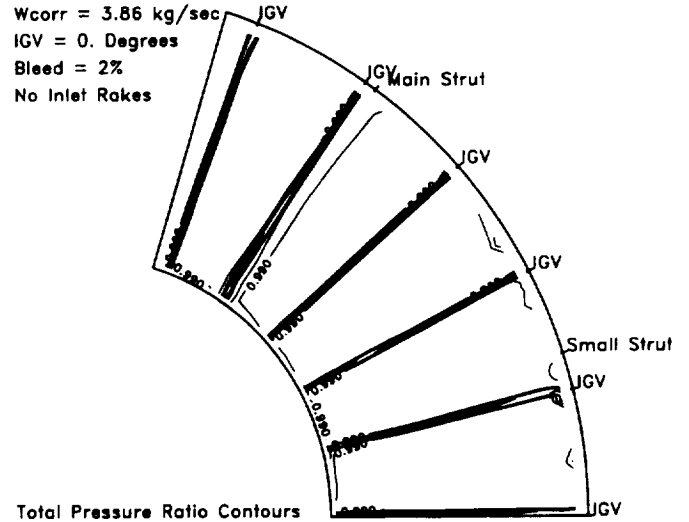


Figure 7a: Total pressure ratio contours, ranging from 0.93 to 0.99 in intervals of 0.01

A capability existed to bleed off the boundary layer with altitude exhaust along the shroud just upstream of the IGV's. Figures 8a-c show the 2% bleed case with no rakes. Comparing the results of the pressure ratio contours to the non-bleed test, a significant decrease in the pressure loss was observed in the tip region. The flow at this condition



**Figure 7b: Exit flow angle contours, ranging from -6 to 8 degrees in intervals of 2 degrees**



**Figure 8a: Total pressure ratio contours, ranging from 0.93 to 0.99 in intervals of 0.01**

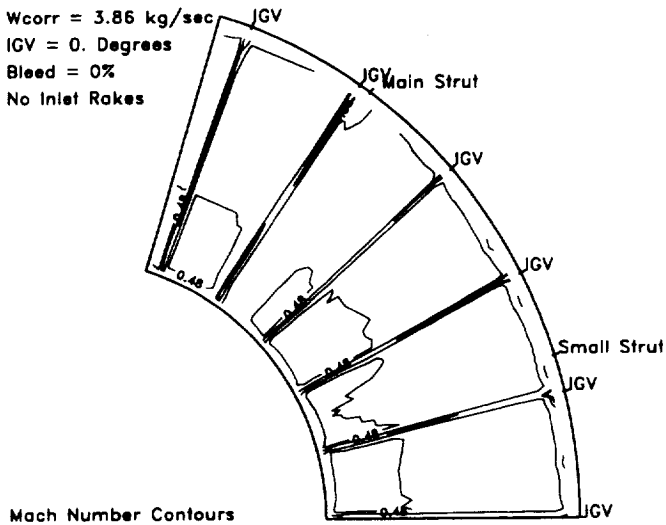


**Figure 7c: Mach number contours, ranging from 0.34 to 0.48 in intervals of 0.02**

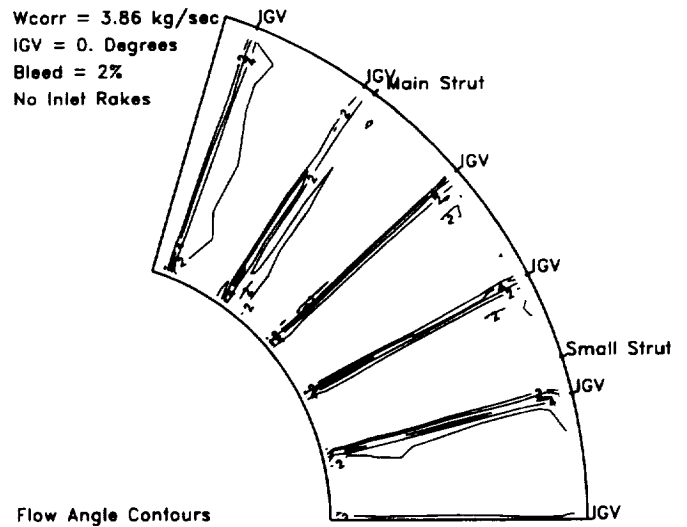


**Figure 8b: Exit flow angle contours, ranging from -6 to 8 degrees in intervals of 2 degrees**

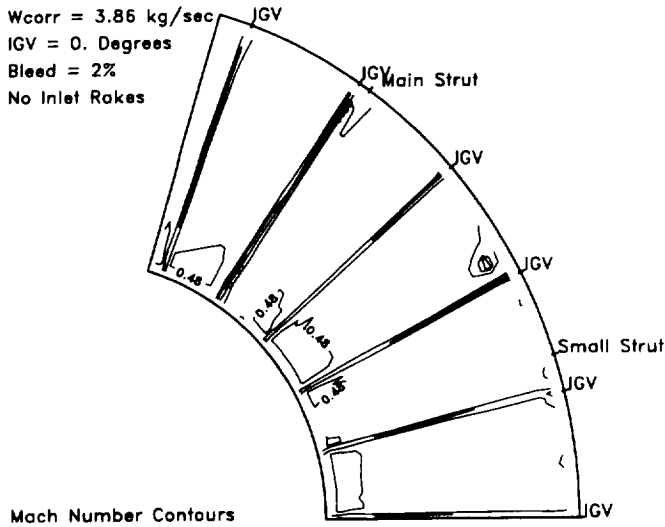


Figure 8c. Mach number contours, ranging from 0.34 to 0.48 in intervals of 0.02

shows that the boundary layer had been successfully removed, only showing the wakes generated by the IGV's, and a small influence of the main strut.

Detailed radial profiles of the flow were taken in regions of core flow. Figure 9 shows the spanwise variation of total pressure ratio, total temperature ratio, flow angle and Mach number, for the 3.86 kg/s, IGV setting angle at 0 degrees, and without bleed flow. The traversing probe total temperature was corrected for Mach number and shown normalized by the inlet plenum total temperature.

Figure 10 shows the spanwise variation of the same parameters with 2% bleed at the shroud. The pressure remains constant to almost 95% of the span, an increase in total pressure over the previous run without bleed. The boundary bleed was significant enough to be used during compressor testing to find out whether the bleed will improve the compressor efficiency or not.

The next set of figures will show the flow with the IGV closed to 30 degrees, and the corrected flowrate reduced to 3.27 kg/s. The flow was surveyed with and without bleed, and with the inlet rakes in place.

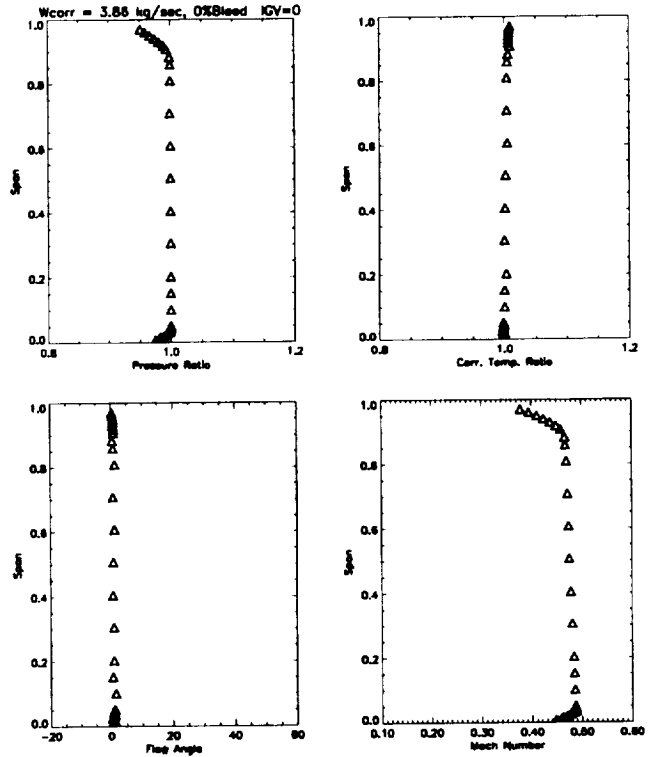


Figure 9. Radial Profiles of the Flow in the Core Region for 3.86 kg/s, no bleed.

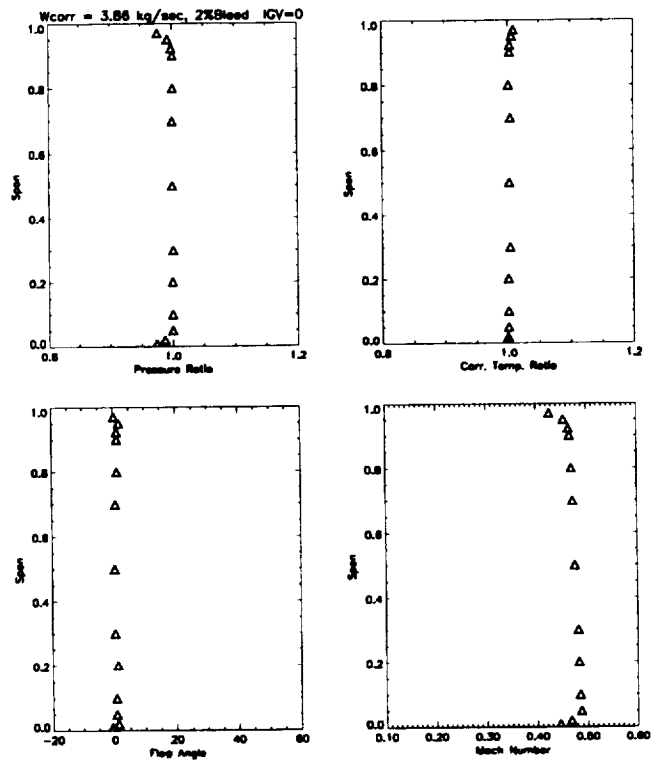


Figure 10. Radial Profiles of the Flow in the Core Region for 3.86 kg/s, 2% bleed.

Figure 11a. shows the total pressure contours at the 30 degree IGV setting without boundary layer bleed. The wakes shed by the inlet guide vanes have moved clockwise away from the IGV locations marked on the plot, and the pressure loss increased significantly from the 0 degree IGV setting. The loss increased to  $\Delta P_t/P_{t,0}$  of 0.85 compared to  $\Delta P_t/P_{t,0}$  of 0.93 for the zero IGV setting. Flow angle contour measurements are shown in Figure 11b, varying between 20 and 40 degrees.

Next, the bleed was set to 4% of mass flow, instead of 2%, to determine the optimum necessary bleed for the compressor test and a survey taken. Figure 12 shows the pressure ratio contours for the 30 degree IGV case and 4% bleed. This reduced the endwall effects, but didn't significantly reduce the overall loss in the system.

Radial profiles at a fixed circumferential location were also taken for the 30 degree IGV setting with and without bleed in the core flow region. Figure 13 shows a comparison of the spanwise variation of total pressure ratio, for two bleeds. As can be seen the loss near the tip endwall region is the only region affected by the bleed.

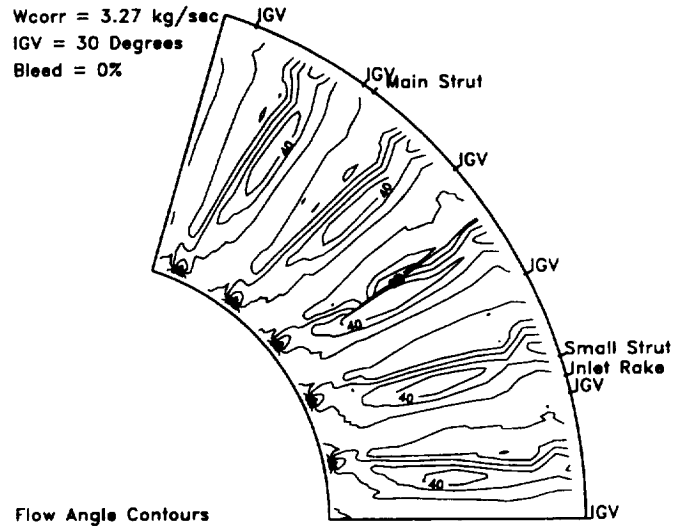


Figure 11b. Exit flow angle contours, ranging from 20 to 40 degrees in intervals of 5 degrees

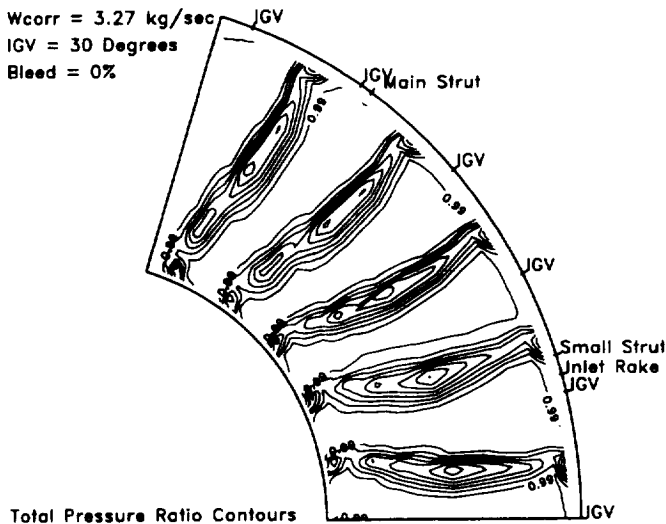


Figure 11a. Total pressure ratio contours, ranging from 0.85 to 0.99 in intervals of 0.02

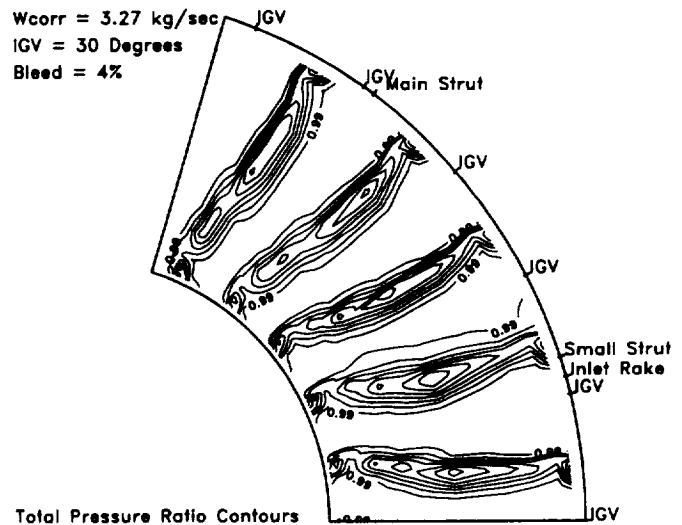


Figure 12. Total pressure ratio contours, ranging from 0.85 to 0.99 in intervals of 0.02

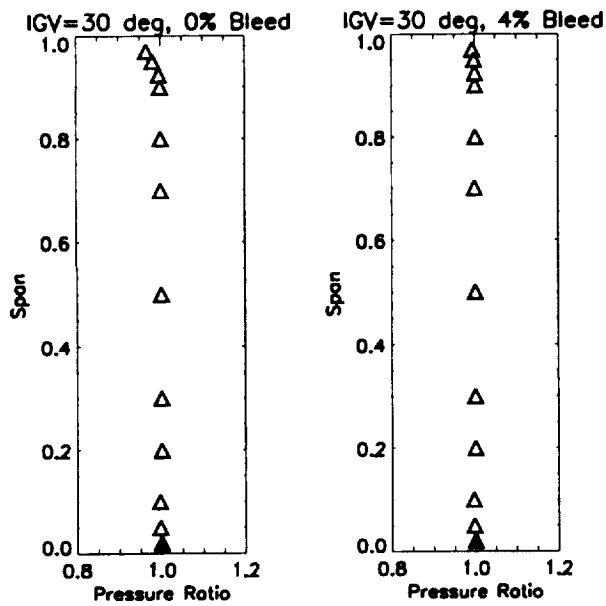


Figure 13. Radial Profile of the Flow in the Core Region for 3.27 kg/s and 30 Degree IGV setting.

The IGV was also placed at 11, 40, and 45 degree setting angles, and surveys were made with and without bleed. The detailed survey data for these IGV angle settings were left out of this report, but will be published later.

#### 4.3 Loss Calculations

From the detailed measurements behind the inlet guide vanes of total pressure data, a spanwise profile of the losses were computed. The losses were computed on both an area averaged and mass averaged basis. For the area average total pressure loss  $\Delta P_t/P_{t,0}$  the integration of pressure in the circumferential direction becomes

$$\frac{\Delta P_t}{P_0}(r) = 1 - \frac{\int_{\theta_1}^{\theta_n} \frac{P_t}{P_0} r dr d\theta}{\int_{\theta_1}^{\theta_n} r dr d\theta} \quad (2)$$

Where  $P_t$  is the total pressure measured behind the inlet guide vane,  $P_0$  is the inlet pressure measured at the plenum,  $r$  is the radial coordinate,  $\theta$  is the circumferential or pitchwise direction of the flow survey. The loss was integrated over a 72 degree sector.

The mass average total pressure loss was determined by the following

$$\frac{\Delta P_t}{P_0}(r) = 1 - \frac{\int_{\theta_1}^{\theta_n} \frac{P_t}{P_0} \rho U r dr d\theta}{\int_{\theta_1}^{\theta_n} \rho U r dr d\theta} \quad (3)$$

where  $U$  is the axial velocity, and  $\rho$  is the density.

Figure 14 shows the radial variation of the loss for the maximum flow rate condition and the IGV setting angle of 0 degrees. The losses were compared with and without bleed and with and without the inlet rake ahead of the IGV. There is a significant change in the pressure loss once the

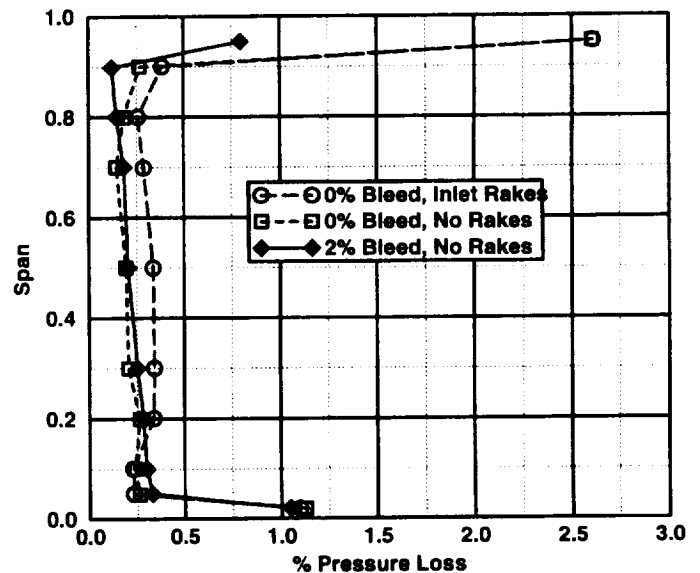


Figure 14. Area Averaged Spanwise Variation of Total Pressure Loss for 0 Degree IGV angle setting.

rake instrumentation was removed. The plot shows an improvement in the loss of pressure in the core flow from the case where the rakes were intruding into the flow. There is a significant decrease in loss at the shroud once the bleed of the boundary layer is applied. At 2% bleed condition, the loss at the 95% span location dropped from 2.6% to less than 1%. The mass averaged total pressure losses were computed to within 0.03% of the area averaged values and therefore not shown.

Figure 15 shows the spanwise variation of pressure loss for the 30 degree vane setting, with and without bleed. Notice the overall increase of the loss from the shroud to midspan, as it increases from about 1% to almost 2.5% at

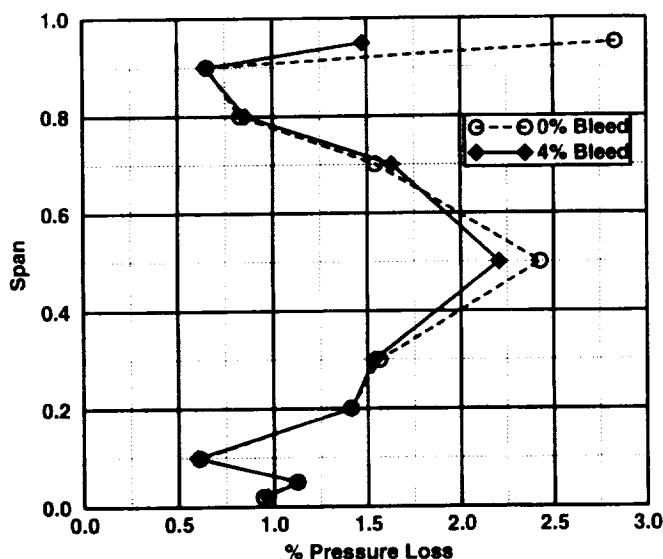


Figure 15. Spanwise Variation of Total Pressure Loss for 30 Degree IGV angle setting.

midspan, and then decreases to just over half percent at 90%span. The endwall losses don't appear to have significantly increased while the midspan losses have dramatically increased. As the flap of the IGV is closed the secondary flow field effects strengthen, migrating the loss down from the tip region and up from the hub. The loss could also have been due to a partially separated boundary layer on the suction side of the airfoil. Future CFD analysis will be required to determine whether the loss is a combination of effects or the single effect mentioned above.

## 5.0 Concluding Remarks

A compressor inlet was designed and tested in the Small Engine Components Test Facility at NASA Lewis Research Center to verify inlet conditions to the compressor. Detailed flowfield measurements were obtained using a miniature flow measuring probe. From the inlet rake measurements, the total conditions into the IGV were found to be within 0.2% of plenum conditions. Since the inlet rakes were a significant loss, the rakes were to be removed during compressor testing. The boundary layer bleed significantly improved the endwall losses near the casing. An optimum 2% bleed was determined to provide substantial loss reduction in the endwall region. Even though there were two sets of support struts, the losses generated from these struts were relatively small. As the IGV flap is closed, the strong secondary flow effects significantly increase the losses in the midspan region of the blade. The off-design performance of the IGV has been well documented with the detailed flow measurements taken.

Detail flow measurements have been taken over several different flow conditions and IGV setting angles with and without bleed. These measurements provide a substantial data base for the small compressor inlet region to be used in future small compressor testing and CFD validation.

## 6.0 Acknowledgments

The author(s) would like to thank the following personnel for contributions to this program: Kevin McCormick and Charlie Martin for assembly and operation of the test hardware. Richard Brokopp, Teresa Gibson and Bob Gronski for maintaining and operating the facility. Bill Stevans for his contribution on the design of a ring traverse probe. Finally, Sue Prahst, co-author, for writing the data reduction program.

## 7.0 References

- [1] Brokopp, R. A. and Gronski, R. S., "Small Engine Components Test Facility Compressor Testing Cell at NASA Lewis Research Center" NASA TM-105685, Presented at the 17th AIAA Aerospace Ground Testing Conference, Nashville, TN, July 1992, pp. 1-11.
- [2] Steinke, R. J., "Design of 9.271-Pressure Ratio Five Stage Core Compressor and Overall Performance for First Three Stages," NASA TP-2597, May 1986.

- [3] Abbott, I. H., and von Doenhoff, A. E., "Theory of Wing Sections," Dover Publications, New York, 1959.
- [4] Sanz, J. M., "Improved Design of Subcritical and Supercritical Cascades Using Complex Characteristics and Boundary-Layer Correction," AIAA Journal, Vol. 22, No. 7, July 1984, pp. 950-956.
- [5] Miller, D. P., and Reddy, D. R., "The Design/Analysis of Flows Through Turbomachinery A Viscous/Inviscid Approach," NASA TM-104447, Presented at the 27th Joint Propulsion Conference, Sacramento, CA, June 1991, pp. 1-10.
- [6] "Flowmeter Computation Handbook", ASME, New York, 1961.

## Appendix A

### Appendix A.1.0 Inlet Flow Region

The inlet flowpaths are shown in Figure A1 and the coordinates are given in the following table below.

**Table A1: Inlet Flowpath Coordinates**

Tip Axial Coordinates (cm)	Tip Radial Coordinates (cm)	Hub Axial Coordinates (cm)	Hub Radial Coordinates (cm)
-119.689	44.797	-119.689	0.000
-111.864	40.398	-38.229	0.000
-104.244	36.395	-38.143	0.377
-96.624	32.656	-38.058	0.753
-89.004	29.184	-37.886	1.092
-81.384	25.991	-37.644	1.388
-73.764	23.070	-37.364	1.652
-66.144	20.431	-37.065	1.895
-58.524	18.082	-36.752	2.116
-50.904	16.019	-36.420	2.311
-45.356	14.706	-36.088	2.507
-43.952	14.399	-35.734	2.655
-42.682	14.130	-35.373	2.790
-41.412	13.868	-35.009	2.914
-40.142	13.616	-34.638	3.016
-38.872	13.370	-34.267	3.119
-37.602	13.134	-33.893	3.219
-36.332	12.908	-32.517	3.472
-35.062	12.689	-31.643	3.596
-33.792	12.479	-30.769	3.672
-32.522	12.275	-29.893	3.721
-31.252	12.082	-28.145	3.742
-29.982	11.897	-26.879	3.742
-28.712	11.722	-26.382	3.741
-27.442	11.559	-26.172	3.741
-26.172	11.394	-25.624	3.741
-25.468	11.311	-25.077	3.741
-24.763	11.229	-24.267	3.740
-24.267	11.176	-22.888	3.740
-24.059	11.150	-22.341	3.739
-23.354	11.074	-21.794	3.739

**Table A1: Inlet Flowpath Coordinates**

Tip Axial Coordinates (cm)	Tip Radial Coordinates (cm)	Hub Axial Coordinates (cm)	Hub Radial Coordinates (cm)
-22.649	10.999	-20.250	3.738
-21.944	10.926	-18.927	3.738
-21.239	10.858	-17.635	3.737
-20.533	10.792	-16.599	3.738
-19.263	10.678	-15.560	3.738
-17.993	10.576	-14.522	3.738
-16.723	10.480	-13.484	3.739
-15.880	10.424	-12.446	3.739
-15.453	10.396	-12.082	3.739
-14.183	10.317	-11.408	3.740
-13.014	10.255	-10.370	3.740
-11.744	10.195	-9.332	3.740
-10.474	10.144	-8.295	3.741
-9.530	10.111	-7.946	3.742
-9.204	10.101	-7.761	3.742
-7.934	10.068	-7.228	3.744
-7.441	10.059	-6.694	3.746
-6.948	10.050	-6.161	3.756
-6.455	10.043	-5.821	3.772
-5.821	10.035	-5.732	3.777
-5.469	10.031	-5.095	3.821
-4.976	10.027	-4.565	3.878
-4.483	10.024	-4.036	3.950
-3.990	10.022	-3.510	4.038
-3.497	10.019	-3.351	4.070
-3.351	10.020	-3.192	4.102
-2.432	10.020	-2.557	4.241
-2.066	10.020	-2.432	4.273
-1.785	10.007	-1.922	4.401
-1.496	9.995	-1.287	4.579
-1.207	9.982	-0.965	4.678
-0.965	9.971	-0.596	4.799
-0.918	9.969	0.000	4.927
-0.635	9.956		
0.000	9.956		

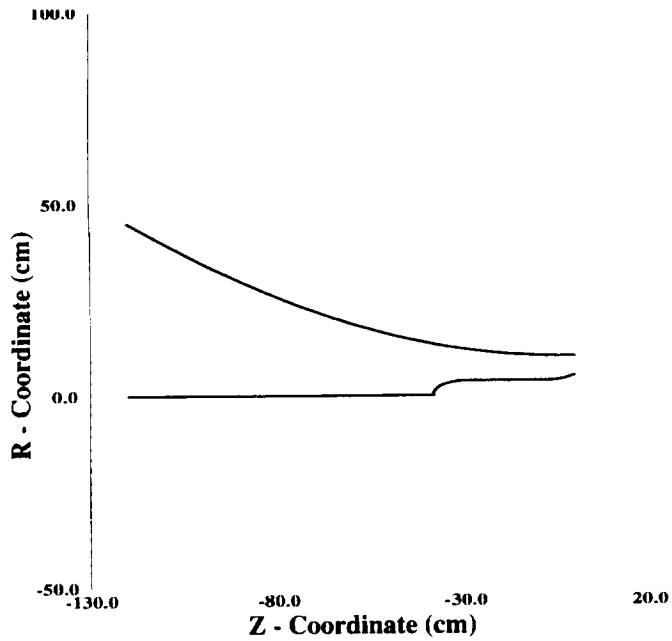


Figure A1: Inlet Flowpath Coordinates

Table A2: NACA0024 Coordinates

x coordinate	y coordinate
0.2894	0.1196
0.3289	0.1198
0.3684	0.1180
0.4078	0.1153
0.4473	0.1118
0.4868	0.1074
0.5908	0.0927
0.7272	0.0679
0.8636	0.0377
1.0000	0.0240

Appendix A.1.1 Small Support Strut Coordinates

The following coordinates are non-dimensional with respect to chord for the forward support strut. Since the small support strut is a symmetrical NACA 0024 airfoil, only the upper surface coordinates are given from the leading edge to the trailing edge of the airfoil. From Abbott and von Doenhoff[3], the thickness can be found from

$$\pm y = \frac{t}{0.20} (0.2969 \sqrt{x} - 0.126x - 0.3516x^2 + 0.2843x^3 - 0.1015x^4) \quad (A.1)$$

where  $t = t_{max}/chord$

Table A2: NACA0024 Coordinates

x coordinate	y coordinate
0.0000	0.0000
0.0131	0.0388
0.0263	0.0535
0.0394	0.0641
0.0920	0.0908
0.1314	0.1026
0.1709	0.1106
0.2104	0.1158
0.2500	0.1188

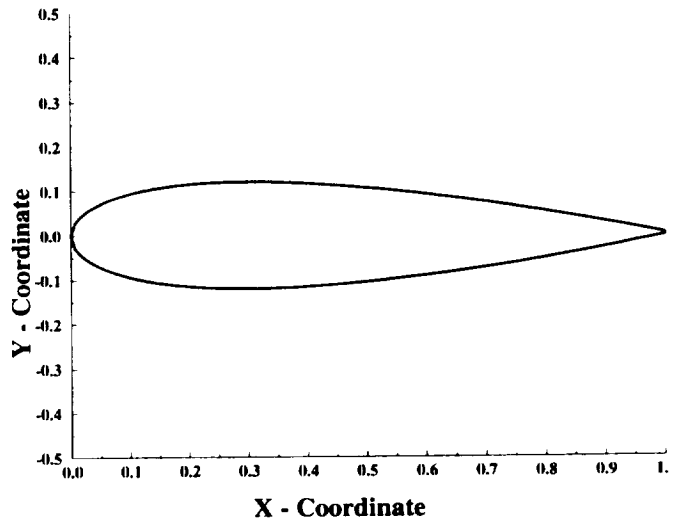


Figure A2: Normalized NACA0024 Airfoil

### Appendix A.1.2 Main Support Strut Coordinates

The following coordinates are non-dimensional with respect to chord for the main support strut. Since the main support strut is also a symmetrical airfoil, only the upper surface coordinates are given from the leading edge to the trailing edge of the airfoil.

**Table A3: Main Strut Coordinates**

x coordinate	y coordinate
0.0000	0.0000
0.0028	0.0068
0.0120	0.0140
0.0256	0.0216
0.0780	0.0396
0.1508	0.0548
0.2584	0.0664
0.3388	0.0696
0.3808	0.0704
0.4448	0.0696
0.5528	0.0636
0.6604	0.0500
0.7688	0.0316
0.8688	0.0168
0.9472	0.0088
0.9920	0.0064
0.9988	0.0060
1.0000	0.0060
1.0000	0.0000

The strut was stacked on the leading edge of the blade along the following stacking line.

$$z_{\text{hub}} = -0.8026 \text{ cm}$$

$$r_{\text{hub}} = 3.7400 \text{ cm}$$

$$z_{\text{tip}} = -4.7778 \text{ cm}$$

$$r_{\text{tip}} = 10.4242 \text{ cm}$$

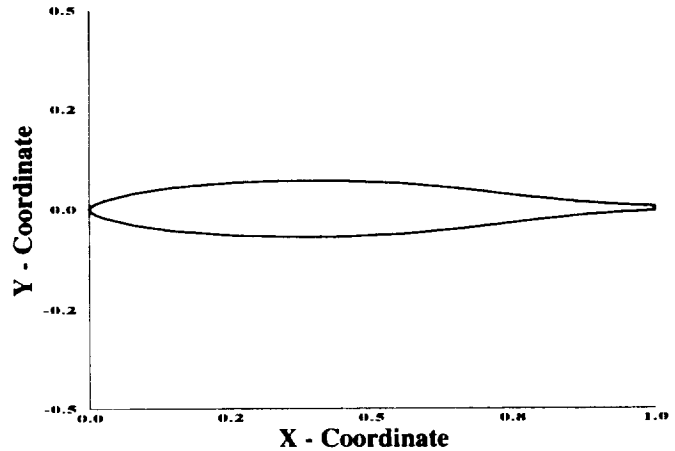


**Figure A3: Normalized Main Support Strut**

### Appendix A.1.3 Inlet Guide Vane Coordinates

The following coordinates are non-dimensional with respect to chord for the inlet guide vane. The IGV consists of a strut and flap. The IGV is also a symmetrical airfoil, only the upper surface coordinates are given from the leading edge to the trailing edge of the airfoil. The strut and flap coordinates are indicated separated in the table

**Table A4: Inlet Guide Vane Coordinates**

x coordinate	y coordinate
0.00000	0.0000
0.00012	0.0017
0.00049	0.0034
0.00108	0.0049
0.00189	0.0063
0.00289	0.0075
0.00406	0.0085
0.00811	0.0098
0.01877	0.0118
0.02971	0.0138
0.04064	0.0159
0.05141	0.0179
0.09292	0.0251
0.1345	0.0313

**Table A4: Inlet Guide Vane Coordinates**

x coordinate	y coordinate
0.1761	0.0365
0.2176	0.0408
0.2592	0.0443
0.2821	0.0453
0.3039	0.0468
0.3434	0.0482
0.3850	0.0489
Flap Geometry	Flap Geometry
0.4267	0.0487
0.4682	0.0481
0.5098	0.0470
0.5514	0.0456
0.5929	0.0436
0.6345	0.0412
0.6762	0.0384
0.7177	0.0351
0.7593	0.0313
0.8010	0.0272
0.8425	0.0225
0.8840	0.0174
0.9257	0.0118
0.9673	0.0059
1.0000	0.0000

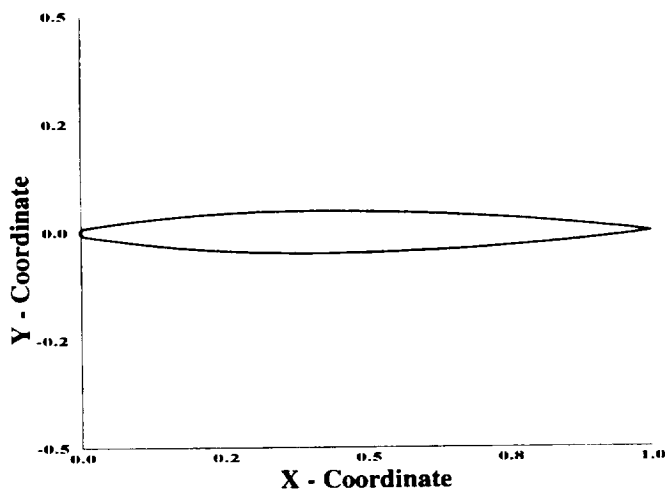


**Figure A4: Normalized Inlet Guide Vane**

**Appendix A.1.4 Main Flowpath Coordinates**

The main flow path coordinate are given below.

**Table A5: Main Flowpath Coordinates**

Tip Axial Coordinates (cm)	Tip Radial Coordinates (cm)	Hub Axial Coordinates (cm)	Hub Radial Coordinates (cm)
0.000	9.956	0.000	4.927
6.701	9.956	0.394	5.009
8.667	9.977	0.966	5.078
9.668	10.065	1.682	5.130
10.675	10.199	6.756	5.130
11.686	10.375	8.158	5.146
12.696	10.590	8.885	5.226
13.702	10.838	9.627	5.351
14.701	11.116	10.381	5.518
15.688	11.419	11.148	5.723
16.660	11.743	11.924	5.965
17.614	12.085	12.709	6.238
18.546	12.439	13.501	6.542
19.452	12.802	14.298	6.873
20.328	13.170	15.099	7.227
21.171	13.538	15.902	7.602
21.978	13.903	16.705	7.996
22.744	14.259	17.507	8.404
23.466	14.604	18.306	8.824
24.141	14.932	19.101	9.253
24.765	15.240	19.890	9.689
		20.671	10.127
		21.444	10.566
		22.205	11.002
		22.955	11.432
		23.690	11.853
		24.410	12.263
		25.112	12.658
		25.796	13.036
		26.871	13.670
		27.396	13.977

**Table A5: Main Flowpath Coordinates**

Tip Axial Coordinates (cm)	Tip Radial Coordinates (cm)	Hub Axial Coordinates (cm)	Hub Radial Coordinates (cm)
		27.937	14.294
		28.478	14.612
		29.018	14.928
		29.550	15.240

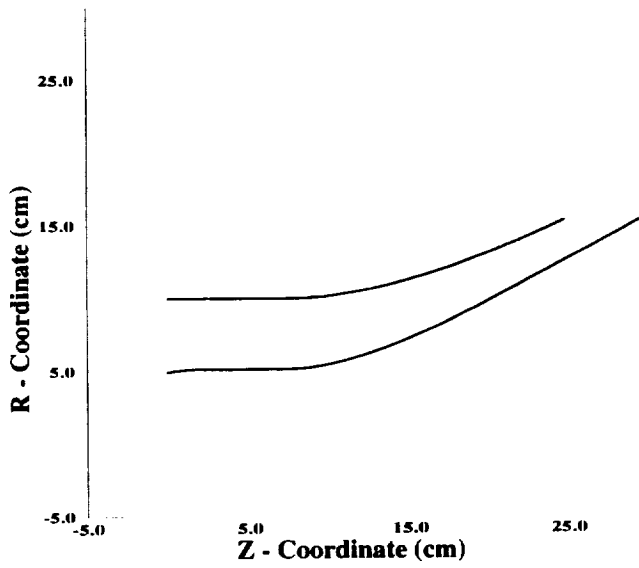


**Figure A5: Main Flowpath Coordinates**



<b>REPORT DOCUMENTATION PAGE</b>			<i>Form Approved</i> OMB No. 0704-0188	
Public reporting burden for this collection of information is estimated to average 1 hour per response, including the time for reviewing instructions, searching existing data sources, gathering and maintaining the data needed, and completing and reviewing the collection of information. Send comments regarding this burden estimate or any other aspect of this collection of information, including suggestions for reducing this burden, to Washington Headquarters Services, Directorate for Information Operations and Reports, 1215 Jefferson Davis Highway, Suite 1204, Arlington, VA 22202-4302, and to the Office of Management and Budget, Paperwork Reduction Project (0704-0188), Washington, DC 20503.				
<b>1. AGENCY USE ONLY (Leave blank)</b>	<b>2. REPORT DATE</b> August 1994	<b>3. REPORT TYPE AND DATES COVERED</b> Technical Memorandum		
<b>4. TITLE AND SUBTITLE</b> Inlet Flow Test Calibration for a Small Axial Compressor Facility Part I—Design and Experimental Results			<b>5. FUNDING NUMBERS</b>  WU-505-62-10	
<b>6. AUTHOR(S)</b>  D.P. Miller and P.S. Prahst				
<b>7. PERFORMING ORGANIZATION NAME(S) AND ADDRESS(ES)</b>  National Aeronautics and Space Administration Lewis Research Center Cleveland, Ohio 44135-3191			<b>8. PERFORMING ORGANIZATION REPORT NUMBER</b>  E-9085	
<b>9. SPONSORING/MONITORING AGENCY NAME(S) AND ADDRESS(ES)</b>  National Aeronautics and Space Administration Washington, D.C. 20546-0001			<b>10. SPONSORING/MONITORING AGENCY REPORT NUMBER</b>  NASA TM-106719	
<b>11. SUPPLEMENTARY NOTES</b> Prepared for the 30th Joint Propulsion Conference cosponsored by AIAA, ASME, SAE, and ASEE, Indianapolis, Indiana, June 27-29, 1994. D.P. Miller, NASA Lewis Research Center and P.S. Prahst, Sverdrup Technology Inc., Lewis Research Center Group, Brook Park, Ohio (work funded by NASA Contract NAS3-25266), presently at NYMA, Inc., Engineering Services Division, 2001 Aerospace Parkway, Brook Park, Ohio 44142. Responsible person, D.P. Miller, organization code 2760, (216) 433-8352.				
<b>12a. DISTRIBUTION/AVAILABILITY STATEMENT</b>  Unclassified - Unlimited Subject Category 07			<b>12b. DISTRIBUTION CODE</b>	
<b>13. ABSTRACT (Maximum 200 words)</b>  An axial compressor test rig has been designed for the operation of small turbomachines. The inlet region consisted of a long flowpath region with two series of support struts and a flapped Inlet Guide Vane. A flow test was run to calibrate and determine the source and magnitudes of the loss mechanisms in the inlet for a highly loaded two-stage axial compressor test. Several flow conditions and IGV angle settings were established in which detailed surveys were completed. Boundary layer bleed was also provided along the casing of the inlet behind the support struts and ahead of the IGV. A detailed discussion of the flowpath design along with a summary of the experimental results are provided in Part I.				
<b>14. SUBJECT TERMS</b>  Axial compressor			<b>15. NUMBER OF PAGES</b> 20	
			<b>16. PRICE CODE</b> A02	
<b>17. SECURITY CLASSIFICATION OF REPORT</b> Unclassified	<b>18. SECURITY CLASSIFICATION OF THIS PAGE</b> Unclassified	<b>19. SECURITY CLASSIFICATION OF ABSTRACT</b> Unclassified	<b>20. LIMITATION OF ABSTRACT</b>	